photonics

MDPI

Article

Sensing Performance of Triple-Band Terahertz Metamaterial Absorber Based on Snowflake-Shaped Resonators

Limin Ma [1,*], Yuhuang Liu [1], Yongkai Zhu [1] and Wenhua Gu [2,*]

[1] College of Automation Engineering, Nanjing University of Aeronautics and Astronautics, Nanjing 211100, China
[2] School of Microelectronics, Nanjing University of Science and Technology, Nanjing 210094, China
* Correspondence: liminma@nuaa.edu.cn (L.M.); guwenhua@njust.edu.cn (W.G.)

Abstract: Terahertz metamaterial absorbers are important functional devices for liquid analyte detection. In contrast to general metamaterial absorbers with single-layer metasurfaces that possess only one resonant mode, a triple-band terahertz metamaterial absorber formed by a single layer of symmetrically arrayed snowflake-shaped resonators was proposed in this study. The simulation results showed that the absorption of the metamaterial absorber reached 97.43% at 0.550 THz, 79.22% at 1.249 THz, and 99.02% at 1.867 THz with narrow resonant peaks. The resonant frequencies were sensitive to the refractive index of the surrounding medium at a fixed analyte thickness, which would play an important role in the performance of the sensor for detecting changes in the surrounding refractive index. The maximum value of the refractive index sensitivity was 137.70 GHz/RIU, 306.25 GHz/RIU, and 473.86 GHz/RIU, with a figure of merit (*FoM*) of 3.14, 2.33, and 6.46, respectively, for refractive index values ranging from 1.0 to 2.2 under three resonant modes. It is worth noting that most of the liquid samples showed a refractive index ranging from 1.0 to 2.0. Furthermore, the identification of peanut oil, carbon disulfide, and turpentine was considered to verify that the proposed terahertz sensor could be used for high-sensitivity liquid detection and has broad development prospects in the field of detecting and sensing.

Keywords: terahertz; metamaterial; multi-band absorber; refractive index sensing

Citation: Ma, L.; Liu, Y.; Zhu, Y.; Gu, W. Sensing Performance of Triple-Band Terahertz Metamaterial Absorber Based on Snowflake-Shaped Resonators. *Photonics* **2022**, *9*, 777. https://doi.org/10.3390/photonics9100777

Received: 19 September 2022
Accepted: 17 October 2022
Published: 19 October 2022

1. Introduction

Liquid analytes are commonly found in the industrial and biomedical fields; thus, the study of liquid sensing is of great significance [1,2]. Due to the unique characteristics of low photon energy and strong penetration possessed by terahertz (THz) waves [3–5], sensors based on THz modulation are recognized as nondestructive inspection tools. These sensors can directly calculate the refractive index of analytes through the noncontact measurement of the changes in the absorption spectrum [6,7]. Microfluidic chips are widely used for the sensing and detection of small amounts of liquid analyte to improve the detection capability [8–10]. However, the sensing accuracy and stability of THz sensors are still limited by the weak response of natural materials to THz waves, which would certainly limit the sensing sensitivity and accuracy for liquid analytes with similar refractive indexes.

Terahertz absorbers are of great significance, and utilizing metamaterials is recognized as a potential path to enhancing the responses to THz waves [11]. Hence, metamaterial absorbers have been studied extensively, with a view to minimizing both the transmission and the reflectivity. The metamaterial absorber with X-shaped resonators reported by Mirzaei et al. [12] could be used to detect DNA in liquid, showing over 85% absorption at 0.85 THz and good selectivity for DNA detection. Janneh et al. [13] reported a metasurface absorber that exhibited perfect absorption, a high quality factor, and a refractive index sensitivity of 187.5 GHz/RIU (gigahertz per refractive index unit). Zhang et al. [10] combined metamaterials with a multi-channel microfluidic chip that achieved a refractive

index sensitivity of 223 GHz/RIU at 1.96 THz. Due to the excellent sensing performance of the THz metamaterial absorber mentioned above, the THz metamaterial absorber is considered a promising device for liquid sensing [13–16]. For instance, in 2020, Wang et al. [17] reported an absorber sensor based on a three-dimensional split-ring resonator (SRR) array and microfluidic channel that could be used as a refractive index sensor with a refractive index frequency sensitivity reaching 379 GHz/RIU. Leaky modes are also an important form of electromagnetic field propagation. Cheng et al. [18] experimentally demonstrated the properties of leaky waves generated inside the air gap between a high-index prism and a metal–dielectric–metal metasurface that could be strongly engineered by the geometrical parameters of the metasurface.

Very recently, multi-band metamaterial absorbers have attracted intense attention due to their potential applications in spectroscopic detection [19]. Compared with traditional single-band metamaterial absorbers, multi-band metamaterial absorbers can realize highly accurate sensing and detection through the multi-point matching of information. Generally, a metamaterial absorber with a single-layer patterned structure shows only one resonant mode. Though a multi-band absorber can be obtained by a multi-layer metasurface, this kind of design leads to a heavy and thick structure. To avoid the thick structure caused by multi-layer metasurfaces, in 2021, Pang et al. [20] designed a dual-band THz metamaterial absorber with a single-layer metasurface whose absorption reached 99% at both 0.387 THz and 0.694 THz. Lan et al. [21] theoretically and experimentally demonstrated a THz biosensor with an intense wave-matter-overlap microfluidic channel. The resonant modes exhibited ultrahigh normalized sensitivities of 0.47/RIU and 0.51/RIU at 0.76 THz and 1.28 THz, respectively. To reduce the strong absorption of THz by water when detecting solution samples and to improve the sensitivity of the sensor, Yang et al. [22] proposed two dual-band THz sensors based on a metamaterial absorber integrated with microfluidics whose refractive index sensitivity could reach 300 GHz/RIU. Lu et al. [23] proposed an ultrathin terahertz dual-band perfect metamaterial absorber using an asymmetric double-split-ring resonator. Yao et al. [24] reported a triple-band metamaterial absorber using a multi-split-electric-ring resonator for sensing applications with maximal sensitivities of 0.119 THz/RIU, 0.248 THz/RIU, and 0.662 THz/RIU. Furthermore, the absorption bands could be continually expanded to the ultra-broadband range using hyperbolic metamaterials (HMMs), which typically comprise a metal–dielectric multilayer structure [25,26].

Therefore, it is very important to find powerful terahertz absorbers that are characterized by strong multi-band terahertz absorption; high quality factors; high compatibility; and a simple, ultra-thin structure consisting of a single-layer metasurface. In this research, we aimed to achieve the above goal using snowflake-shaped resonators. This study demonstrates a novel and simple design for a triple-band THz metamaterial absorber formed by a patterned metallic layer and a metallic ground plane separated by a dielectric layer. The designed THz metamaterial absorber showed three resonant modes that exhibited high absorption values of 97.43% at 0.550 THz, 79.22% at 1.249 THz, and 99.02% at 1.867 THz. The quality factor of the absorber was 26.01, 17.83, and 58.04, respectively, indicating extremely sharp absorption peaks. The absorption mechanism of the three resonant modes was explored. Furthermore, the sensing performance of the proposed absorber was investigated in terms of the surrounding refractive index. It was found that the maximum value of the refractive index sensitivity S was 473.86 GHz/RIU and the maximum FoM was 6.46 for a refractive index ranging from 1.0 to 2.2 at the resonant frequency of f_3. The proposed THz absorber with these superior performance indicators could be implemented in the field of label-free sensing and non-contact detection.

2. Structures and Methods

So far, great efforts have been devoted to broadening the frequency range of the electromagnetic response of metastructures. The most straightforward approach is to superimpose different resonant modes in the system [27]. Inspired by the shape of a snowflake, which possesses branches of different sizes and distributions, Figure 1a,b show schematic

diagrams of the triple-band THz metamaterial absorber, which comprises a sandwich structure of a metasurface top layer resting on the dielectric substrate and a bottom layer of a continuous metallic plane. The topside metasurface is composed of periodically arrayed snowflake-shaped cells, as shown in Figure 1c. The material of both the top and the bottom layers was chosen to be copper (Al), due to its excellent electrical conductivity. The material used for the intermediate dielectric layer was polytetrafluoroethylene (PTEE), whose permittivity is $\varepsilon = 2.1$.

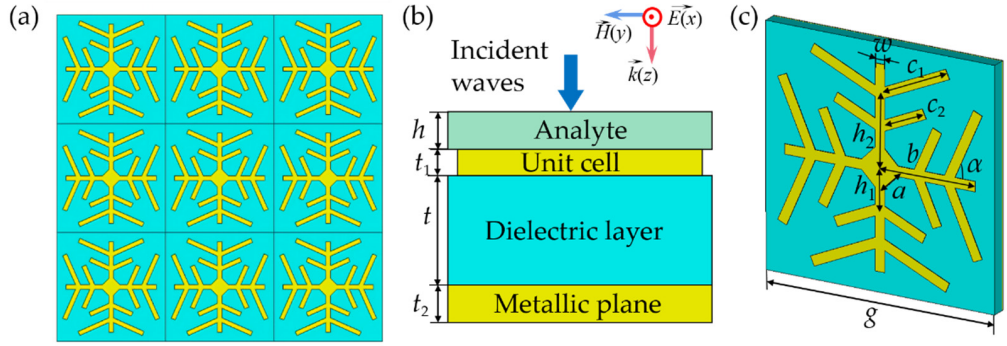

Figure 1. (**a**) Vertical view and (**b**) side view of the proposed triple-band THz metamaterial absorber. (**c**) Perspective view of the snowflake-shaped unit cell.

We implemented a careful design and optimization process involving full-wave simulations using the commercial electromagnetic solver CST Studio Suite 2019 to determine the geometric parameters of the metamaterial absorber shown in Figure 1b,c, which were as follows: the period of the cells $g = 120$ µm; the line-width of cells $w = 5$ µm; the length of the center square $a = 8$ µm; the length of the main branch of each snowflake-shaped cell $b = 50$ µm; the length of the two groups of sub-branches on each main branch, $c_1 = 45$ µm and $c_2 = 30$ µm, respectively; the distance from the sub-branches to the center, $h_1 = 16.95$ µm and $h_2 = 32.77$ µm, respectively; and the angle between the main branch and the auxiliary branch $\alpha = 45°$. The thickness of the intermediate dielectric layer $t = 8$ µm, the thickness of the top layer $t_1 = 0.3$ µm, and the thickness of the bottom continuous Al layer $t_2 = 2$ µm were set to be higher than the skin depth to ensure that the absorber worked in the free transmission mode. The proposed structure was simulated using periodic boundary conditions in the x and y directions with $P_x = P_y = P$. A plane beam polarized along the x-direction was vertically incident on the absorber, as shown in Figure 1b, and periodic boundary conditions were used in the x and y directions. Furthermore, transmission and reflection were calculated under far-field conditions to reveal the physical mechanisms.

3. Results and Discussion

3.1. Structural Design of the Triple-Band THz Metamaterial Absorber

The absorption (A) could be calculated by

$$A = 1 - R - T \tag{1}$$

$$R = |S_{11}|^2 \tag{2}$$

$$T = |S_{21}|^2 \tag{3}$$

where T and R are the transmission and reflection, respectively, and S_{11} and S_{21} are the reflection coefficient and transmission coefficient, respectively. Since the thickness of the continuous Al layer was greater than the skin depth, the transmission of the proposed absorber was suppressed ($T = 0$), so the absorption (A) could be expressed as $A = 1 - R$ [28]. The simulated absorption and reflection spectra of the proposed absorber at normal incidence are shown in Figure 2. It is obvious that the proposed absorber had three resonant modes at the frequency range of 0.2 to 1.8 THz. The resonant frequencies and the corre-

sponding absorption values were as follows: f_1 = 0.550 THz, $A(f_1)$ = 97.43%; f_2 = 1.249 THz, $A(f_2)$ = 79.22%; and f_3 = 1.867 THz, $A(f_3)$ = 99.02%. Triple-band effective absorption was achieved. The full width at half maximum (FWHM) values were FWHM(f_1) = 21.14 GHz, FWHM(f_2) = 70.05 GHz, and FWHM(f_3) = 58.04 GHz, indicating that the absorption spectra were narrow. The quality factor (Q factor) of the absorber was defined as:

$$Q = \frac{f}{FWHM} \tag{4}$$

where f is the resonant frequency. The Q factors were $Q(f_1)$ = 26.01, $Q(f_2)$ = 17.83, and $Q(f_3)$ = 58.04, indicating that the absorption peaks were extremely sharp.

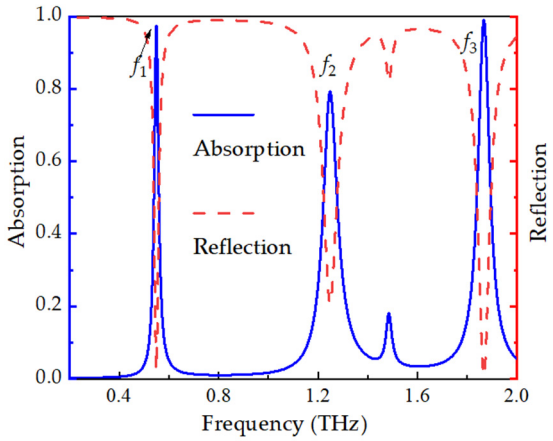

Figure 2. Absorption and reflection spectra of the triple-band THz metamaterial absorber.

Based on the interaction between the incident terahertz waves and the metamaterial absorber, the as-designed metamaterial absorber could still maintain an excellent terahertz absorption performance at an oblique TEM wave incidence. The angular dependence of the absorption performance was investigated, as depicted in Figure 3. The absorption spectrum was nearly independent of the incident angle below 60° for TE polarization, as shown in Figure 3a. Meanwhile, the metamaterial absorber exhibited a high quality factor for all resonance modes, even when the incident angle was increased to 60° for both TE and TM polarization.

3.2. Absorption Mechanism of Triple-Band THz Metamaterial Absorber

In order to gain insight into the absorption mechanism of the absorber and the characteristics of the resonant modes, the distribution of electromagnetic field and surface currents on the top of the snowflake-shaped unit cell were illustrated for a TE-polarized wave with normal incidence. The spatial distributions of the electric field for the three resonant modes, shown in Figure 4, indicated that the snowflake-shaped structure could stimulate strong absorption resonance and produce a strong electric field located near the sidewalls of the branches of the snowflake structure, which could effectively excite surface plasmon resonances (SPRs) in the unit cells [29]. Figure 4a shows that the electric field was mainly concentrated at both sub-branch groups (c_1 and c_2) and the apex of the main branches along the y-axis at resonant frequency f_1 = 0.550 THz. The electric field was mainly focused on the outer sub-branches (c_1) along the x-axis at resonant frequency f_2 = 1.249 THz, as shown in Figure 4b. In the simulation results depicted in Figure 4c, the electric field was obviously concentrated in the inner sub-branches (c_2) along the x-axis at resonant frequency f_3 = 1.867 THz. It is worth noting that the resonant modes were excited by the SPRs at different locations in the snowflake-shaped unit cell.

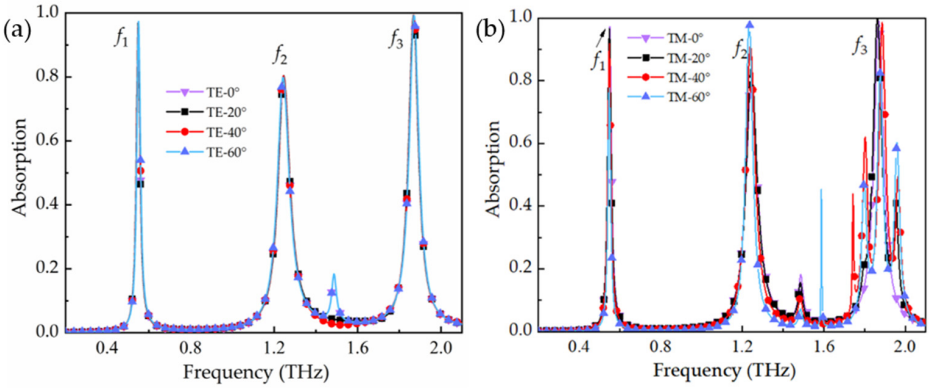

Figure 3. Terahertz absorption in the case of TEM waves incident at different angles from 0° to 60° for (**a**) TE polarization and (**b**) TM polarization.

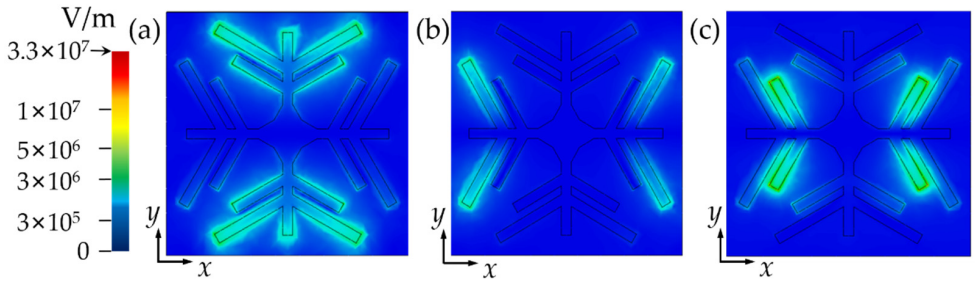

Figure 4. Electric field distributions at the three resonant frequencies: (**a**) f_1 = 0.550 THz, (**b**) f_2 = 1.249 THz, and (**c**) f_3 = 1.867 THz.

Figure 5 shows the magnetic field distribution results of the simulation that included field monitors at the corresponding resonant frequencies f_1, f_2, and f_3. The magnetic field was mainly gathered around the main branches and the sub-branches in the y direction at resonant frequency f_1 = 0.550 THz, while it was concentrated around the outer and inner sub-branches c_1 and c_2 in the x direction at resonant frequency f_2 = 1.249 THz and f_3 = 1.867 THz, respectively. The simulated surface currents on the top of the unit cell under the three resonant modes were illustrated for a linearly TE-polarized wave with a normal incidence (Figure 6). In the case of f_1 = 0.550 THz, most of the currents were primarily confined at the edge of the branches in the y direction (Figure 6a). At f_2 = 1.249 THz and f_3 = 1.867 THz, the currents were observed to behave similarly to those in the previous scenario, being concentrated at different positions in the outer and inner sub-branches, respectively, in the x direction (Figure 6b,c). Due to the symmetry of the unit cell, the electric field, magnetic field, and induced surface currents at the surface had the same distributions for both TE and TM waves [30].

3.3. Sensing Characteristics of Triple-Band THz Metamaterial Absorber

Figure 7a–c show the absorption of the proposed THz metamaterial absorber under different analytes (refractive indexes n changing from 1 to 2.2) with an analyte thickness of h = 5 µm, as shown in Figure 1b. It can be seen that the absorption changed as the refractive index n varied for all three resonant modes. For instance, the absorption at resonant frequency f_1 = 0.550 THz dropped from 97.43% to 1.05% when the analyte refractive index n changed from 1 to 2.2, as shown in Figure 7a. Furthermore, the resonant frequency gradually redshifted for all three resonant modes when the analyte refractive index n changed from 1 to 2.2 with an interval of 0.2, as shown in Figure 7. In order to determine the sensing performance of the proposed THz metamaterial absorber, we analyzed the relationship between the variation in the refractive index n and the frequency shifting for the three resonant modes (Figure 8), which was confirmed to represent linear fitting.

Moreover, the sensitivity S could be defined as the slope of the fitted line according to the following formula [31]:

$$S = \frac{\Delta f}{\Delta n} \tag{5}$$

where Δf is the variation in resonant frequency caused by changing the refractive index Δn. The sensitivities for the three resonant modes were $S(f_1)$ = 97.94 GHz/RIU, $S(f_2)$ = 216.50 GHz/RIU, and $S(f_3)$ = 377.34 GHz/RIU.

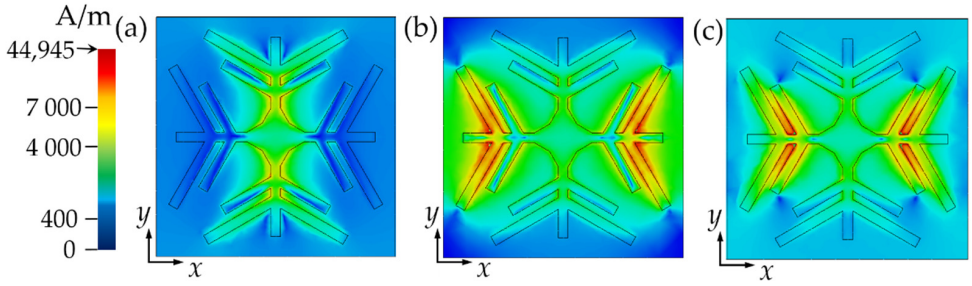

Figure 5. Magnetic field distributions at the three resonant frequencies: (**a**) f_1 = 0.550 THz, (**b**) f_2 = 1.249 THz, and (**c**) f_3 = 1.867 THz.

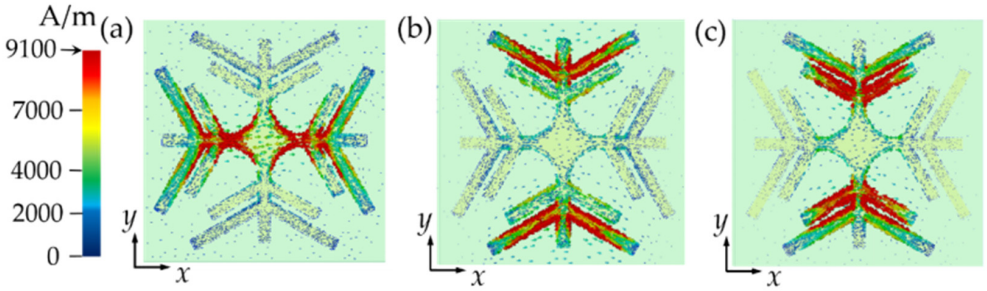

Figure 6. Top view of the simulated surface currents at the three resonant frequencies: (**a**) f_1 = 0.550 THz, (**b**) f_2 = 1.249 THz, and (**c**) f_3 = 1.867 THz.

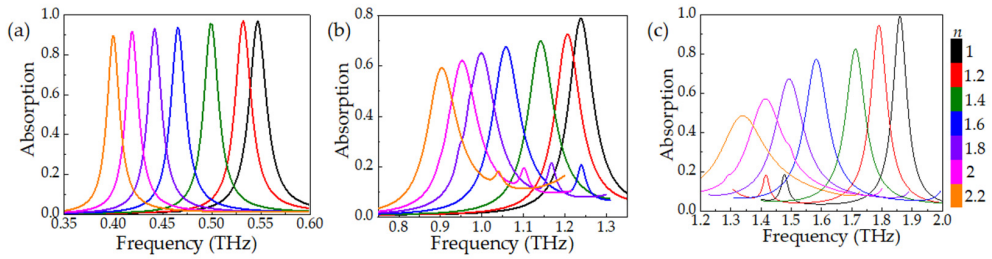

Figure 7. Absorption spectra of the THz metamaterial absorber when the refractive index of analyte n changed from 1 to 2.2 under the three resonant frequencies: (**a**) f_1, (**b**) f_2, and (**c**) f_3.

The volume of analytes also affected the sensitivity S of the proposed sensor. Figure 9a–c show simulated resonant frequency shifting maps as functions of different analyte thickness values h ranging from 5 to 25 µm for the three resonant modes. Figure 9d shows the influence of the analyte thickness h on the sensitivity of the sensor. The refractive index sensitivity at resonant frequencies f_1 and f_2 achieved the maximum value of $S(f_1)$ = 137.70 GHz/RIU and $S(f_2)$ = 306.25 GHz/RIU when the analyte thickness h was 20 µm. The maximum value of the refractive index sensitivity at the highest resonant frequency $S(f_3)$ = 473.86 GHz/RIU appeared when h = 15 µm. However, the refractive index sensitivity S decreased as the analyte thickness h continued to increase, which was caused by two phenomena. On the one hand, the refraction and dissipation of terahertz waves in the liquid analyte changed as the analyte thickness continually increased, which

led to variations in the absorption spectra. On the other hand, the refractive index sensitivity of an absorption sensor with a certain structure is limited to an ultimate value. Hence, the refractive index sensitivity did not continuously increase or even decrease when the thickness of the analyte was higher than 15~20 μm. Considering the refractive index sensitivity S, it could be concluded that the optimum analyte thickness h was 15 or 20 μm. In addition to sensitivity S, we also used the figure of merit (FoM) as another coefficient for assessing the sensing performance of the proposed absorber, which could be defined as:

$$FoM = \frac{S}{FWHM} \tag{6}$$

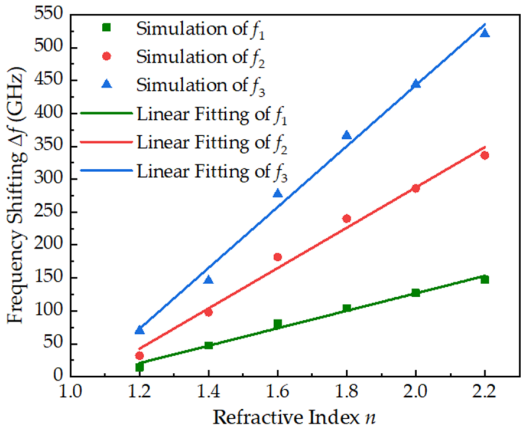

Figure 8. The functional relationship between resonant frequency shifting and the refractive index of the analytes n for three resonant modes with an analyte thickness h = 5 μm.

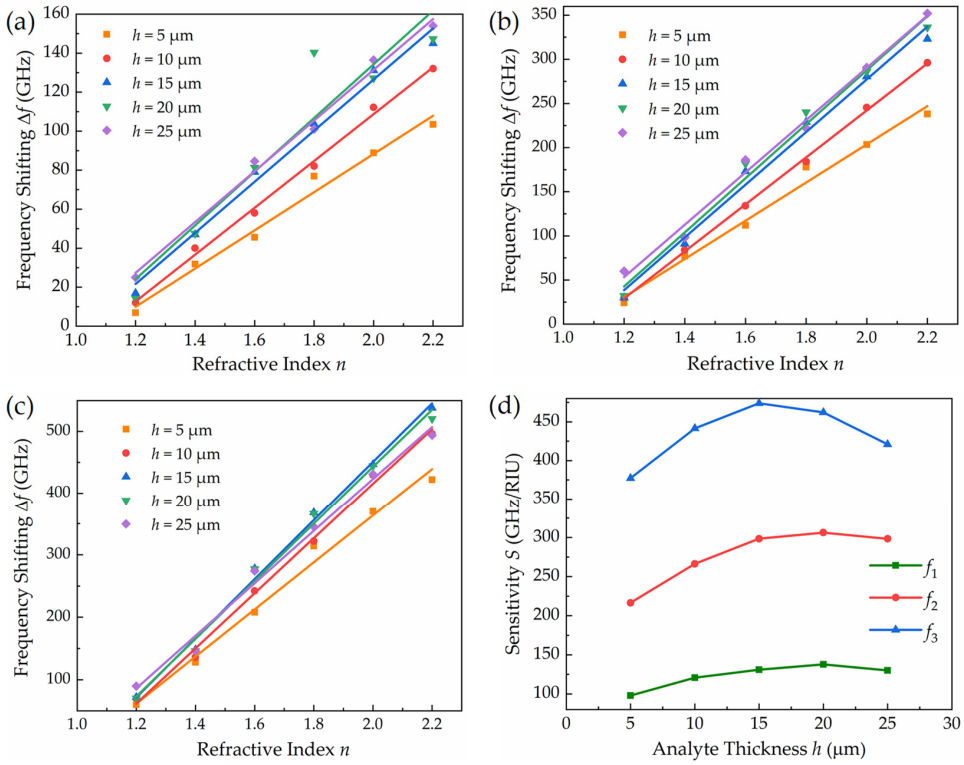

Figure 9. Resonant frequency shifting maps as functions of analyte thickness at the three resonant frequencies (**a**) f_1, (**b**) f_2, and (**c**) f_3. (**d**) Influence of the analyte thickness on the sensitivity of the sensor.

The FoM at resonant frequencies f_1, f_2, and f_3 was $FoM(f_1)$ = 3.14, $FoM(f_2)$ = 2.33, and $FoM(f_3)$ = 6.46, respectively, with an analyte thicknes h = 20 μm. Table 1 shows

the absorption, sensitivity, Q factor, and *FoM* of our device and the designs proposed in previous works. It can be seen that the sensing performance of our device was either superior or comparable to that of the other reported works.

Table 1. Comparison of absorption, sensitivity, Q factor, and *FoM* of the resonant modes in the present study and in previous works.

References	Resonant Frequency (THz)	Absorption	Sensitivity (GHz/RIU)	Q Factor	*FoM*
Ref. [10]	2.06	/	72	/	1.58
Ref. [17]	0.79	98.8%	379	53	25
Ref. [21]	0.378	99%	39.5	28.1	2.94
	0.694	98%	85	29.3	12.5
Ref. [22] Design A	0.64	99%	32	10.3	/
	0.88	99%	44	15	/
Ref. [22] Design B	0.6	96.8%	30	9.7	/
	0.86	96.8%	43	14.8	/
Ref. [23]	4.48	98.6%	/	/	/
	4.76	98.5%	/	/	/
Ref. [24]	0.64	/	119	/	/
	1.94	/	248	/	/
	2.67	/	662	/	/
This paper	0.55	97.43%	137.70	26.01	3.14
	1.249	79.22%	306.25	17.83	2.33
	1.867	99.02%	473.86	58.04	6.46

In order to verify the liquid detection performance of the proposed THz sensor, we analyzed the absorption spectra (Figure 10) of the absorber with and without the analyte coating, which was set as carbon disulfide with a refractive index n = 1.628. We chose turpentine with a permittivity of 2.2, carbon disulfide with a permittivity of 2.6, and peanut oil with a permittivity of 3.0 as the three different liquid analytes. There are two ways to model an analyte in CST Studio Suite 2019 simulation software. The first is to directly choose the corresponding material in the material library. The second is to set the permittivity of the analyte ε according to $n = \varepsilon^{1/2}$ for non-magnetic materials, where n is the refractive index of the analyte. Figure 11a–c show the simulated absorption spectra results for these liquid analytes with a thickness of h = 20 µm. As can be seen, it was easy to distinguish the different liquid analytes according to the locations of the absorption peaks at the resonant frequencies f_1, f_2, and f_3. Hence, the three liquid analytes could be identified using the proposed THz sensor. The locations of the resonant frequencies f_1, f_2, and f_3 for the different liquid analytes are shown in Figure 11d. When the analyte was peanut oil, the resonant frequencies f_1, f_2, and f_3 were located at 0.450, 1.016, and 1.522 THz, respectively, according to the simulation results shown in Figure 11d. Compared with the refractive index n = 1 of the surrounding air, the resonant frequency shift was Δf_1 = 96.5 GHz, Δf_2 = 222.86 GHz, and Δf_3 = 337.29 GHz, respectively. Based on the calculated results for the refractive index sensitivity $S(f_1)$ = 137.70 GHz/RIU, $S(f_2)$ = 306.25 GHz/RIU, and $S(f_3)$ = 462.16 GHz/RIU, the refractive index of the liquid analytes n could be derived by the following formulas:

$$n_1 = \Delta n_1 + 1 = \frac{\Delta f_1}{S(f_1)} + 1 \quad (7)$$

$$n_2 = \Delta n_2 + 1 = \frac{\Delta f_2}{S(f_2)} + 1 \quad (8)$$

$$n_3 = \Delta n_3 + 1 = \frac{\Delta f_3}{S(f_3)} + 1 \quad (9)$$

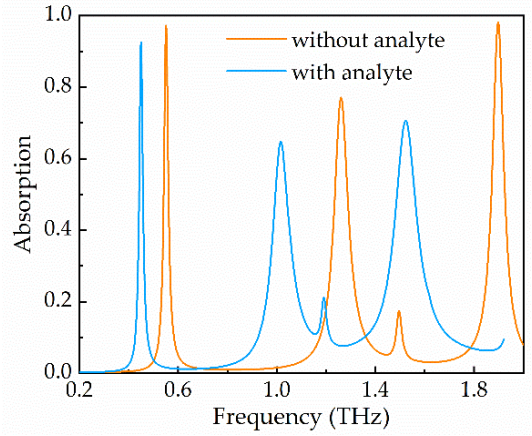

Figure 10. The absorption spectra of the absorber with and without the analyte coating.

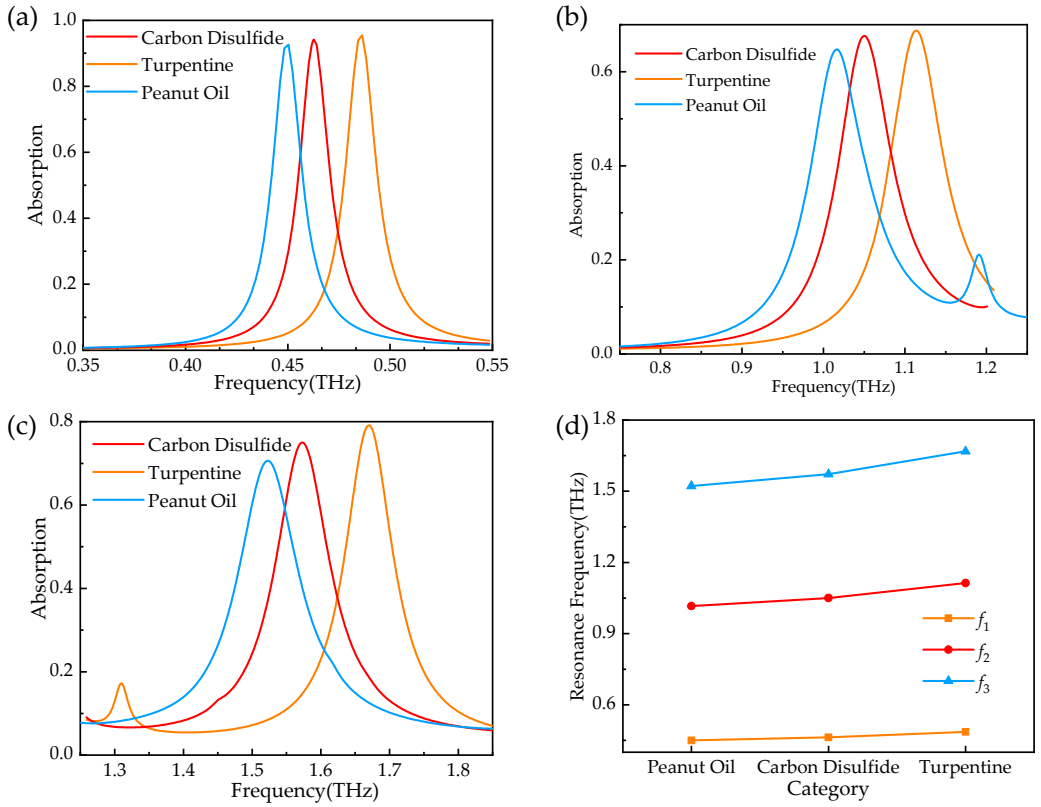

Figure 11. (**a**) Simulated absorption spectra results for the three resonant frequencies (**a**) f_1, (**b**) f_2, and (**c**) f_3. (**d**) Locations of the resonant frequencies f_1, f_2, and f_3 for different liquid analytes at frequencies ranging from 0.2 to 1.8 THz.

Based on Equations (7)–(9), the calculated refractive index of peanut oil was n_1 = 1.701, n_2 = 1.727, and n_3 = 1.712 according to the different resonant modes. Similarly, the calculated refractive index of carbon disulfide was n_1 = 1.620, n_2 = 1.627, and n_3 = 1.616 according to the different resonant modes, while the calculated refractive index of turpentine was n_1 = 1.440, n_2 = 1.471, and n_3 = 1.434. Since the known refractive indexes of peanut oil, carbon disulfide, and turpentine are 1.715, 1.628, and 1.472, respectively, it can be seen that the refractive index n_2 calculated by the resonant frequency f_2 was more accurate than those calculated by the resonant frequencies f_1 and f_3, due to the larger deviation introduced by the linear fitting of the refractive index sensitivity for the resonant frequencies f_1 and f_3 compared to f_2.

4. Conclusions

In conclusion, we presented a novel triple-band snowflake-shaped metamaterial absorber design based on a sandwich structure. The absorption at the three resonant frequencies was 97.43%, 79.22%, and 99.02%, respectively. Moreover, the sensing properties of the proposed THz absorber were demonstrated with different analyte thicknesses, ranging from 5 to 25 μm, and different refractive indexes, ranging from 1.0 to 2.2, for the three resonant modes. The maximum value of the refractive index sensitivity was 137.70 GHz/RIU, 306.25 GHz/RIU, and 473.86 GHz/RIU for the three resonant frequencies. The identification of peanut oil, carbon disulfide, and turpentine indicated that compared with the resonant frequencies f_1 and f_3, the resonant frequency f_2 was closer to the exact refractive index of the surroundings.

Author Contributions: L.M. wrote the paper; Y.L. conceived and designed the simulation; Y.Z. and W.G. conducted the editing and review. All authors have read and agreed to the published version of the manuscript.

Funding: This research was funded by the China Postdoctoral Science Foundation (Grant No. 2020TQ0152); Natural Science Foundation of Jiangsu Province (No. BK20190405); National Natural Science Foundation of China (No. 61905112, 61905114); National Key Research and Development Program (2018YFB2003803); Fundamental Research Foundation for the Central Universities (NZ2020005, NT2021013); and Postgraduate Research and Practice Innovation Program of NUAA (xcxjh20210339).

Institutional Review Board Statement: Not applicable.

Informed Consent Statement: Not applicable.

Data Availability Statement: Not applicable.

Conflicts of Interest: The authors declare no conflict of interest.

References

1. Kayal, S.; Shaw, T.; Mitra, D. Design of miniaturized highly sensitive liquid sensor at microwave frequency. *Int. J. RF Microw. Comput.-Aided Eng.* **2020**, *30*, e22387. [CrossRef]
2. Ma, X.X.; Chen, K.X.; Wu, J.Y.; Wang, L.F. Low-Cost and Highly Sensitive Liquid Refractive Index Sensor Based on Polymer Horizontal Slot Waveguide. *Photonic Sens.* **2020**, *10*, 7–15. [CrossRef]
3. Romain, X.; Baida, F.; Boyer, P. Extended Malus' Law with THz metallic metamaterials for sensitive detection with giant tunable quality factor. *Phys. Rev. B* **2016**, *5*, 045407. [CrossRef]
4. Su, Z.X.; Yin, J.B.; Zhao, X.P. Terahertz dual-band metamaterial absorber based on graphene/MgF2 multilayer structures. *Opt. Express* **2015**, *23*, 1679–1690. [CrossRef]
5. Sun, S.L.; He, Q.; Hao, J.M.; Xiao, S.Y.; Zhou, L. Electromagnetic metasurfaces: Physics and applications. *Adv. Opt. Photonics.* **2019**, *380*, 380–479. [CrossRef]
6. Sotsky, A.B.; Nazarov, M.M.; Miheev, S.S.; Sotskaya, L.I. Sensitivity of Reflecting Terahertz Sensors of Aqueous Solutions. *Tech. Phys.* **2021**, *66*, 305–315. [CrossRef]
7. Hossain, B.; Rahaman, E.; Mondal, H.S.; Kabiraj, S.; Raihan, M. Design and optimization of the perilous chemical sensor in the terahertz frequency range. *Mater. Today Proc.* **2020**, *43*, 3720–3724.
8. Tang, Q.; Liang, M.; Lu, Y.; Wong, P.K.; Wilmink, G.J.; Zhang, D.; Xin, H. Microflfluidic devices for terahertz spectroscopy of live cells toward lab-on-a-chip applications. *Sensors* **2016**, *16*, 476. [CrossRef]
9. Yeo, L.Y.; Chang, H.C.; Chan, P.Y.; Friend, J.R. Microflfluidic devices for bioapplications. *Small* **2011**, *7*, 12–48. [CrossRef]
10. Zhang, R.; Cherr, Q.M.; Liu, K.; Chen, Z.F.; Li, K.D.; Xu, J.B. Terahertz Microfluidic Metamaterial Biosensor for Tiny Volume Liquid Samples. In Proceedings of the 2018 43rd International Conference on Infrared, Millimeter, and Terahertz Waves (IRMMW-THz), Nagoya, Japan, 9–14 September 2018; pp. 1–2.
11. Barroso, R.H.; Malpica, W. An Overview of Electromagnetic Metamaterials. *IEEE Lat. Am. Trans.* **2020**, *18*, 1862–1873. [CrossRef]
12. Mirzaei, S.; Green, N.G.; Rotaru, M.; Pu, S.H. Detecting and identifying DNA via the THz backbone frequency using a metamaterial-based label-free biosensor. In *Terahertz, RF, Millimeter, and Submillimeter-Wave Technology and Applications X*; Proc SPIE: Bellingham, WA, USA, 2017; Volume 12, pp. 101031–101038.
13. Janneh, M.; Marcellis, A.D.; Palange, E.; Tenggara, A.T.; Byun, D. Design of a metasurface-based dual-band Terahertz perfect absorber with very high Q-factors for sensing applications,ptics Communications. *Opt. Commun.* **2018**, *416*, 152–159. [CrossRef]
14. Saadeldin, A.S.; Hameed, M.F.O.; Elkaramany, E.M.A.; Obayya, S.S.A. Highly Sensitive Terahertz Metamaterial Sensor. *IEEE Sens. J.* **2019**, *19*, 7993–7999. [CrossRef]

15. Mayani, M.G.; Herraiz-Martínez, F.J.; Domingo, J.M.; Giannetti, R. Resonator-Based Microwave Metamaterial Sensors for Instrumentation: Survey, Classification, and Performance Comparison. *IEEE Trans. Instrum. Meas.* **2021**, *70*, 9503414. [CrossRef]
16. Bhardwaj, A.; Pratap, D.; Srivastava, K.V.; Ramakrishna, S.A. Highly Sensitive Permittivity Sensor Using an Inhomogeneous Metamaterial Cylindrical Waveguide. *IEEE Sens. J.* **2021**, *21*, 9120–9127. [CrossRef]
17. Wang, X.; Wang, J.L. Terahertz Metamaterial Absorber Sensor Based on Three-Dimensional Split-Ring Resonator Array and Microfluidic Channel. *Acta Optica Sinica* **2020**, *19*, 19–26.
18. Cheng, Q.Q.; Zhang, C.S.; Yu, D.; Chen, L.; Xie, J.Y.; Zang, X.F.; Shkurinov, A.; Zhu, Y.M.; Zhang, S.L. Manipulation of the terahertz leaky wave by metal–dielectric–metal metasurface. *Appl. Phys. Express* **2019**, *12*, 072008. [CrossRef]
19. Wang, B.X.; Wang, G.Z.; Sang, T. Simple design of novel triple-band terahertz metamaterial absorber for sensing application. *Phys. D Appl. Phys.* **2016**, *46*, 165307. [CrossRef]
20. Pang, H.Z.; Wang, X.; Wang, J.L.; Wang, Z.L.; Liu, S.Y.; Tian, H.Q. Sensing characteristics of dual band terahertz metamaterial absorber sensor. *Acta Phys.* **2021**, *70*, 168101. [CrossRef]
21. Lan, F.; Luo, F.; Mazumder, P.; Yang, Z.Q.; Meng, L.; Bao, Z.Q.; Zhou, J.; Zhang, Y.X.; Liang, L.X.; Shi, Z.J.; et al. Dual-band refractometric terahertz biosensing with intense wave-matter-overlap microfluidic channel. *Biomed. Opt. Express* **2019**, *10*, 3789–3799. [CrossRef]
22. Yang, J.P.; Wang, M.C.; De, H.; Kang, Y.; Li, Z.R.; Liu, Q.C.; Xiong, L.; Wu, Z.X.; Qu, W.W.; Shang, L.P. Dual-Band Terahertz Sensor Based on Metamaterial Absorber Integrated Microfluidic. *Acta Optica Sinica* **2021**, *41*, 2428001.
23. Lu, T.G.; Zhang, D.; Qiu, P.; Lian, J.; Jing, M.; Yu, B.; Wen, J. Ultrathin Terahertz Dual-Band Perfect Metamaterial Absorber Using Asymmetric Double-Split Rings Resonator. *Symmetry* **2018**, *10*, 293. [CrossRef]
24. Yao, Y.; Li, S.; Zhu, L.; Wu, F.; He, X.; Jiang, J. Multi-band terahertz metamaterial absorber for sensing application. *Integr. Ferroelectr.* **2018**, *190*, 149–155. [CrossRef]
25. Yin, X.; Chen, L.; Li, X. Ultra-Broadband Super Light Absorber Based on Multi-Sized Tapered Hyperbolic Metamaterial Waveguide Arrays. *J. Light. Technol.* **2015**, *33*, 3704–3710. [CrossRef]
26. Yin, X.; Long, C.; Li, J.H.; Zhu, H.; Chen, L.; Guan, J.G.; Li, X. Ultra-wideband microwave absorber by connecting multiple absorption bands of two different-sized hyperbolic metamaterial waveguide arrays. *Sci. Rep.* **2015**, *5*, 15367. [CrossRef] [PubMed]
27. Fan, R.H.; Xiong, B.; Peng, R.W.; Wang, M. Constructing Metastructures with Broadband Electromagnetic Functionality. *Adv. Mater.* **2019**, *32*, 1904646. [CrossRef]
28. Wang, Z.Y.; Ou, Y.H.; Wang, S.Y.; Meng, Y.Z.; Wang, Z.; Zhai, X.; Wang, L.L.; Xia, S.X. Ultrahigh-Q Tunable Terahertz Absorber Based on Bulk Dirac Semimetal with Surface Lattice Resonance. *Photonics* **2022**, *9*, 22. [CrossRef]
29. Yan, F.; Li, L.; Wang, R.; Tian, H.; Liu, J.; Liu, J.; Tian, F.; Zhang, J. Ultrasensitive Tunable Terahertz Sensor with Graphene Plasmonic Grating. *J. Light. Technol.* **2019**, *12*, 1103–1112. [CrossRef]
30. Zhang, C.; Chen, Q.; Yang, J.; Zhao, J.; Cui, T.J. Broadband metamaterial for optical transparency and microwave absorption. *Appl. Phys. Lett.* **2017**, *110*, 143511. [CrossRef]
31. Xiao, W.F.; Ou, Y.H.; Wang, S.Y.; Wang, S.; Meng, Y.Z.; Xiang, Z.; Xia, S.X.; Wang, L. Ultra-high sensitivity terahertz sensor based on a five-band absorber. *J. Opt.* **2022**, *24*, 055102. [CrossRef]